Novel inorganic scintillating detectors and their applications in small animal irradiators: measurements and Monte Carlo simulations

Byrne, Kevin, Alharbi, Majed, O'Keeffe, Sinead, Kleefeld, Christoph, Bazalova-Carter, Magdalena, et al.

Kevin Byrne, Majed Alharbi, Sinead O'Keeffe, Christoph Kleefeld, Magdalena Bazalova-Carter, Mark Foley, "Novel inorganic scintillating detectors and their applications in small animal irradiators: measurements and Monte Carlo simulations," Proc. SPIE 11354, Optical Sensing and Detection VI, 113540U (1 April 2020); doi: 10.1117/12.2555551

SPIE.

Event: SPIE Photonics Europe, 2020, Online Only, France

Novel inorganic scintillating detectors and their applications in small animal irradiators: Measurements and Monte Carlo simulations

Kevin Byrne[a], Majed Alharbi[a], Sinead O'Keeffe[b], Christoph Kleefeld[c], Magdalena Bazalova-Carter[d], Mark Foley[a]

[a]School of Physics, National University of Ireland, Galway, Ireland;
[b]Optical Fibre Sensors Research Centre, University of Limerick, Ireland;
[c]University Hospital Galway, Ireland;
[d]Department of Physics and Astronomy, University of Victoria, British Columbia, Canada.

ABSTRACT

In the field of radiation therapy, optical fiber dosimeters (OFD) offer several advantages over conventional dosimeters for real-time dosimetry. Their sensing tips can be small in size affording them the potential for high spatial resolution capabilities. In previous work, a novel inorganic scintillating detector (ISD) based on Gadolinium Oxysulfide (gadox) was fabricated for *in vivo* optical fiber dosimetry of conformal small animal irradiators. The performance of this detector was evaluated for 40 and 80 kVp imaging beams and the 220 kVp therapy beam of the Small Animal Research Platform (SARRP). The purpose of this study was to use a validated Monte Carlo (MC) model of the SARRP to investigate (i) dose absorption in the ISD active volume and (ii) dose perturbation by the inorganic scintillating phosphor volume. A comparison was also drawn between the perturbation by the gadox phosphor and a ZnS-based phosphor. The gadox-based detector was seen to cause high levels of dose perturbation in the radiation field, leaving significant dose shadows in the irradiated media. The use of ZnS:Ag phosphor reduces the perturbations with just over half as much dose absorbed relative to the gadox phosphor. An optimized ISD design which utilizes the higher light yield of the less perturbing ZnS:Ag phosphor to allow for a smaller high-density active volume, and significantly mitigating kV dose perturbation, has been proposed.

Keywords: Inorganic scintillating detector, Monte Carlo, optical fiber dosimeter, scintillator, small animal irradiator.

INTRODUCTION

Preclinical studies are essential to reducing human exposure to harmful substances and treatments. Animal models have been used for decades to provide an insight into disease processes and to assist in the development of new strategies to prevent, mitigate and cure disease through preclinical trials. In the fields of radiobiology and radiation oncology, mice – utilized for their cost effectiveness and versatility – are now a standard component of oncology research. As imaging and irradiation techniques in clinical radiation oncology advance, researchers utilizing small animal irradiator technology must strive to replicate human treatment capabilities and consequential clinical relevance. Small animal irradiators generally operate at kilovoltage energies and employ small field sizes ($\leq 1 \times 1$ cm^2), making high spatial-resolution dosimetry vital in ensuring high accuracy and precision for treatment verification and quality assurance.

Optical fiber dosimeters (OFDs) offer several advantages over conventional dosimeters for real-time dosimetry. Their sensing tips can be small in size, affording them high spatial resolution capabilities and close proximity to tumor sites. They can be also operated within intense magnetic fields, making them suitable for use in MRI-guided irradiations. The sensing tip of an OFD contains a scintillating material that fluoresces in the optical range upon exposure to ionizing radiation. The emitted light then propagates along an optical fiber core to a readout device such as a photomultiplier tube or multi-pixel photon counting module, where the signal is converted into electric charge. OFDs are typically terminated with plastic scintillating detectors (PSDs) due to their near water-equivalence, energy independence and short response time. However, they suffer from especially low light output at low beam energies, which can introduce noise related issues

Optical Sensing and Detection VI, edited by Francis Berghmans, Anna G. Mignani, Proc. of SPIE
Vol. 11354, 113540U · © 2020 SPIE · CCC code: 0277-786X/20/$21 · doi: 10.1117/12.2555551

in the signal output. Inorganic scintillating detectors (ISDs), on the other hand, have far superior light output to PSDs and longer radiation lifetimes. Although they are known to suffer from dependencies, especially with respect to energy, they present an attractive option for small field dosimetry of kilovoltage beams once fully characterized.

Our recent work on the topic of radiation dosimetry has been predominantly for clinical treatment applications in the megavoltage range. A novel design was constructed utilizing Terbium-doped Gadolinium Oxysulfide (gadox) inorganic scintillating phosphor (Gd_2O_2S:Tb) and its dosimetric performance was evaluated in comparison to commercially available detectors[1–4]. The contribution of Cerenkov radiation to the signal generated by the detector was also investigated[3]. Monte Carlo (MC) modelling in our group has so far focused predominantly on linear accelerator treatment head modelling in megavoltage applications from a variety of vendors, including Siemens[5–8], Varian[9,10] and Elekta[11–13].

More recently, several novel ISDs were fabricated for *in vivo* optical fiber dosimetry of small animal irradiators[14]. An initial evaluation of some key dosimetry characteristics was carried out for the 40 and 80 kVp imaging beams and 220 kVp therapy beam of the Small Animal Research Platform (SARRP) at the University of Victoria, BC, Canada. Following this, with the present study, we have expanded our MC investigations to model the kilovoltage beam used in small animal irradiators. The Gd_2O_2S:Tb phosphor from our previous studies had proven to be a strong choice of scintillating material, primarily because of the very large signal intensities observed. However, with an effective atomic number (Z_{eff}) of approximately 60[15], radiation interaction processes will be dominated by the photoelectric effect in the SARRP beam energy range (≤ 225 kV). In addition, with a density (ρ) of 7.44 g.cm^{-3} the extent to which the phosphor can attenuate and scatter impinging radiation is likely significant. Such perturbation of dose in the active volume may exist at an unacceptable level in these low energy radiation fields and creating a dose shadow in the media behind the sensing tip (with respect to the beam direction), disqualifying the technology from *in vivo* applications.

We use a validated MC model[16] of the SARRP to investigate the distribution of dose within a virtual phantom made up of a virtual model of our gadox-based detector immersed in a volume of water under irradiation from a 10 x 10 mm^2 field size, 220 kVp beam. The purpose of this study is to come to a better understanding of (i) the distribution of absorbed dose in the high-density active volume of novel ISD designs (ii) any local increases in absorbed dose surrounding the ISD sensing-tip and (iii) the extent of dose perturbation due to high absorption in the inorganic phosphor.

Silver-activated Zinc Sulfide (ZnS:Ag) phosphor – which was investigated previously as a lower Z_{eff} and ρ and, therefore, less perturbing option of inorganic scintillating phosphor – has demonstrated a limited ability to measure the profiles of small, low energy radiation fields due to incompatibility with the detector geometry. It is well known that the scintillation efficiency of ZnS:Ag is high, with reports of light yield up to 100 000 photons per MeV[17,18], even in comparison Gd_2O_2S:Tb (up to 70 000 photons per MeV)[19]. However, it is particularly opaque to its own scintillations. Typically, thicknesses greater than about 25 mg.cm^{-2} yield no additional signal due to phosphor absorbing its own luminescence[18], a phenomenon known as the secondary inner filter effect[20]. It follows that when reducing the active volume dimensions of a ZnS:Ag scintillating detector to increase spatial resolution capabilities and inhibit dose perturbation effects, the length (i.e. thickness) can be reduced to around 60 μm with little to no loss in signal. As such, a virtual model of an improved ZnS-based detector concept which considers the necessity for a shallow active volume length is also discussed.

METHODOLOGY

2.1 SARRP Monte Carlo modelling

The SARRP modelled in this study operates with 220 kVp (therapy) and 40, 50, 60, 70, and 80 kVp (imaging) beam energies with focal spot sizes of 3.0 and 0.4 mm for therapy and imaging beams, respectively[21]. Previously, the MC software package BEAMnrc[22,23], which was developed at the National Research Council (NRC), Canada using the EGS code, was used to model the SARRP and perform radiation transport simulations[24]. A schematic of the MC model of the SARRP is shown in Figure 1, illustrating the geometries used to approximate the actual components of the system. This model has been validated for depth dose and profile measurements of the 220 kVp therapy beam in both homogenous and heterogenous phantoms[16]. This model was used to simulate beam production, filtration and collimation in the SARRP for 8×10^7 particle histories of the 220 kVp beam with collimation to 10×10 mm^2 field size impinging on a number of dose-scoring phantoms.

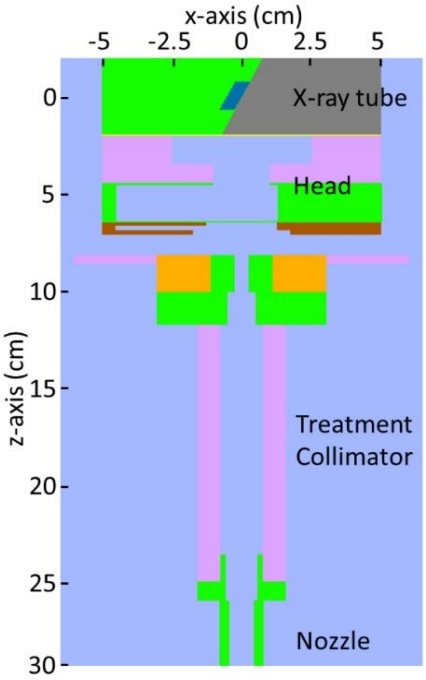

Figure 1. 3-D representation of the detector model used in DOSXYZnrc phantom[16].

2.2 Monte Carlo dose calculations

The radiation field simulated in BEAMnrc was used to calculate the distribution of dose in rectilinear voxel phantoms created using DOSXYZnrc[25]. Materials were created using the density correction files provided with the EGSnrc package, which are based on the International Commission on Radiation Units and Measurements Report 37[26]. The EGSnrc code was used to generate the PEGS4 cross-section data for scintillator materials[1]. The virtual model of the gadox-based sensing tip (the distal 3 mm of fiber containing scintillating material) phantom (Figure 2, right), comprised of 0.25 mm cube voxels of Gd_2O_2S, PMMA and polyethylene, configured with a maximum dimension of 2.25, 2.25 and 3 mm in the x, y and z directions, respectively. It is intended to replicate the actual detector fabricated and evaluated in our previous study (Figure 2, left). In order to understand the perturbation effects of such a high-density active volume in radiation field sizes typical of small animal irradiations, this virtual detector geometry was positioned in a cuboidal volume of water to simulate *in vivo* conditions.

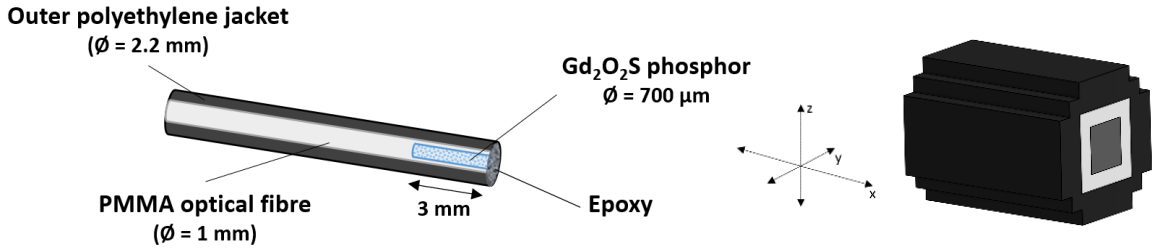

Figure 2. Schematic of the gadox-based detector[14] (left) and a 3-D representation of the virtual sensing tip model created in DOSXYZnrc (right).

A simpler two-layered model, with an upper 1 was used to provide a comparison between the dose absorbed in gadox and ZnS based active volumes. Two detector phantoms were created (one using gadox, the other ZnS) with 1 mm cube voxels. The phosphor voxels were placed in the center of the irradiation field at a depth of 5 cm with a layer of PMMA-polyethylene hybrid material placed just over them. A water only phantom was also included in this comparison.

2.3 Dose distribution analysis

STATDOSE[27] was used to generate profiles and depth-dose curves through selected coordinates of the dose scoring phantoms. In this manuscript the y-coordinate was set to zero. Dose profiles were taken along the x-direction at different depths of the 0.25 mm cube sensing tip model to illustrate the most extreme perturbation of dose. Each voxel dose value in the x-profile plots were normalized to the average dose value between -0.4 and +0.4 cm at the surface of the water to enable a convenient comparison of dose deposited between different layers of interest throughout the phantom. Depth-dose curves were generated along the z-axis at the center of the irradiation field (0, 0) for the 1 mm cube gadox and ZnS-based detector phantoms and compared to a phantom containing only water. Each voxel dose value of the depth-dose curves is normalized to the value of the voxel at the surface of the water for each respective simulation.

RESULTS AND DISCUSSION

Beam profiles illustrating dose along the x-axis at different depths in the gadox detector-containing water phantom are shown in Figures 3 to 6. Figure 3 depicts the dose profile of the surface layer of the water phantom alongside profiles taken one layer above and below the sensing tip volume at depths of 1.975 and 2.225 cm, respectively. Although there is a significant dose shadow in the latter, note that there is no obvious increase in localized dose in the former.

Figure 4 illustrates the dose profiles through the three layers of the Gd_2O_2S core. A very sharp increase in absorbed dose in seen, particularly in the first layer (z = 2.075 cm). With an average relative dose over 38 times the surface dose to water in the phantom, this result represents a significant limitation of the material for *in vivo* applications.

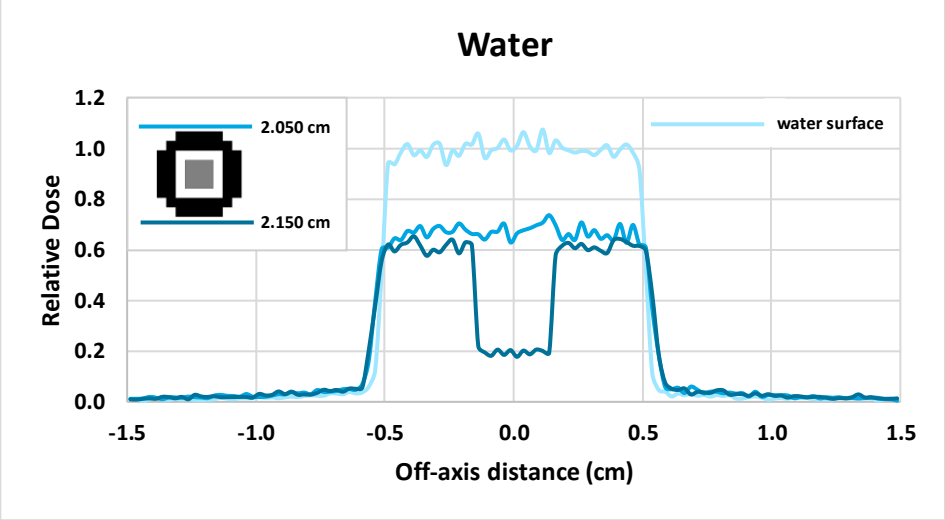

Figure 3. x-axis dose profiles taken at depths containing only water – at the surface, just above and just below the simulated sensing tip model volume.

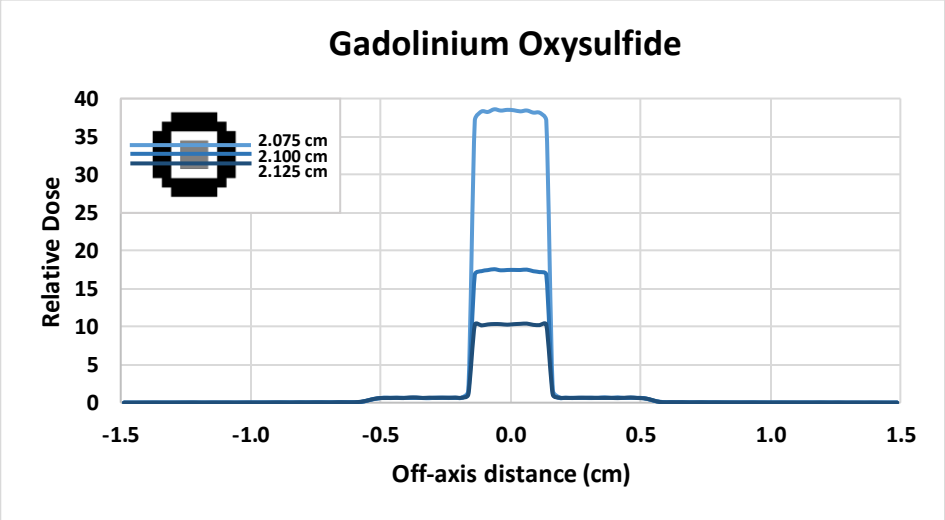

Figure 4. x-axis dose profiles taken at each of the three layers of the detector phantom containing the gadox core.

Dose profiles through the layers of PMMA 'before' and 'after' the gadox active volume (with respect to the beam path) are plotted in Figure 5. There is likely two causes of the obvious overdosing seen in the upper layer (z = 2.050 cm). Firstly, an inherent increase in deposited dose due to PMMA's higher ρ and Z_{eff}, and secondly, backscattering from the surface layer of the Gd_2O_2S core. The inherent increased absorption due to higher ρ and Z_{eff}, in comparison to water, also quells the expected dose shadow in the lower layer at 2.150 cm.

In Figure 6 the two 'entrance' layers of polyethylene at depths of 2.000 and 2.025 cm are plotted alongside the lower 'exit' layers at depths of 2.175 and 2.200 cm. As expected, the exit layers of polyethylene exhibit significant dose shadows due to the 3 mm length of highly absorbing Gd_2O_2S phosphor proceeding it in the beam path. Yet, there is no overdosing present in the upper layers. The underdosing seen is consistent with polyethylene's lower ρ and Z_{eff} with respect to water and its presence is indicative of a low number of backscattered photons escaping out of the fiber core and into the polyethylene jacket.

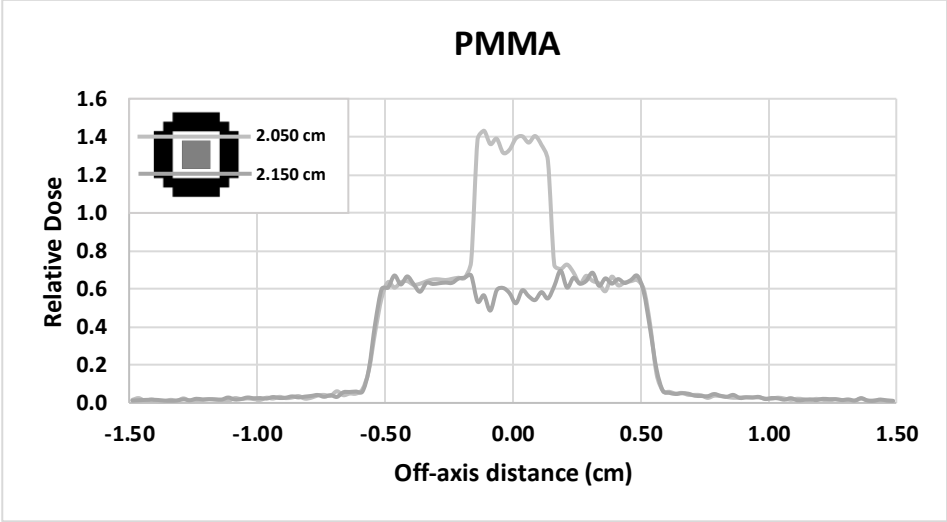

Figure 5. x-axis dose profiles taken at the depths of the PMMA layers just above and below the gadox core.

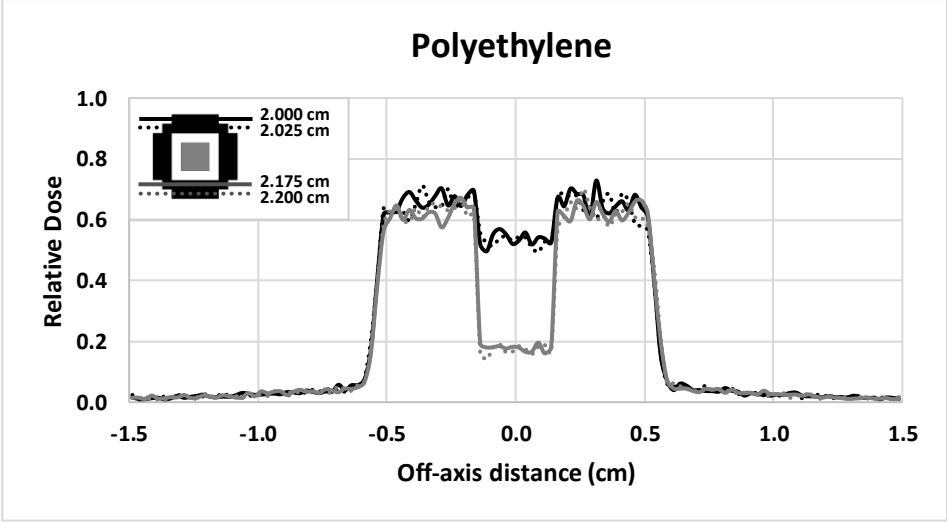

Figure 6. x-axis dose profiles taken at the four depths containing polyethylene – two entrance layers above and two exit layers below the PMMA core.

The average percentage error of the voxel doses between -0.4 and +0.4 cm was 3.1% at the surface of the water. As the maximum voxel dose is over 38 times that dose to the surface of the water, the average percentage error value of the dose to voxels receiving greater than 50% of the maximum voxel dose (< 0.5%) is skewed, as only the average percentage error of the gadox-filled voxels used in this calculation. To reduce the average percentage error (i.e. noise) on the above profiles to within a target of 1%, we would increase the number of particle histories by a factor of about 10.

Figure 7 below depicts PDD profiles taken along the z-axis at the center of the irradiation field for the 1 mm cube gadox, ZnS and water phantoms. The three phosphor voxels in the gadox and ZnS phantoms absorbed 28.3 and 16.1 times as much dose as water voxels in the same location in the water phantom, respectively.

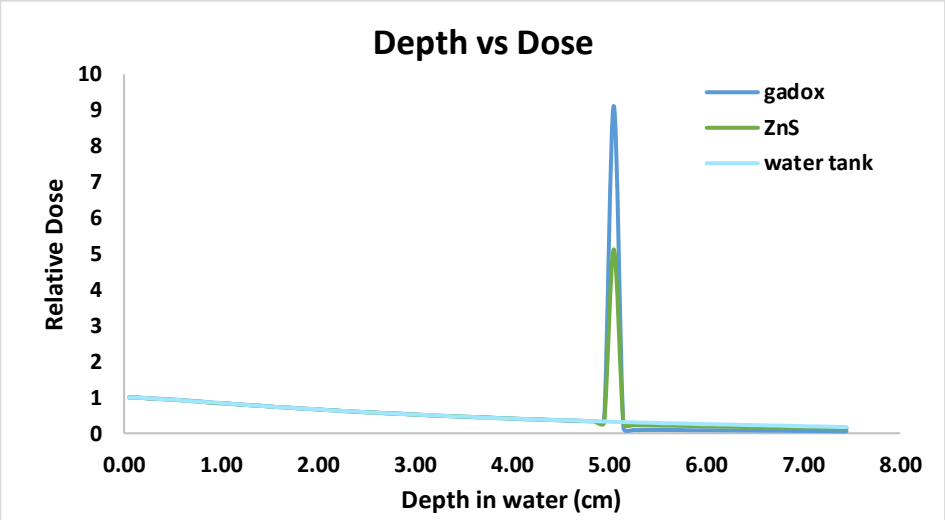

Figure 7. Depth-dose curve for the 1 mm cube gadox, ZnS and water phantoms.

Considering our focus on small field kilovoltage beams in small animal irradiators, the perturbation effects associated with the current gadox-based prototype are unsuitable for the application, insofar as it would take both a significant reduction of the high density volume geometry and a reduction of ρ and Z_{eff} of the scintillator to provide value to the application. Given the median particle size of ZnS-based scintillating phosphors is on the order of 10 μm, and the absorption length of ZnS phosphor is around 60 μm, a fully optimized ZnS:Ag scintillator-based ISD design length would be on the order of 50-100 μm. A100 μm long active volume adhered to the end of a 1 mm optical fiber would decrease the overall volume of the high density component of the ISD design by a factor of around 150 and could be modelled using a 0.1 mm cube voxel phantom. Scoring dose in a 0.1 mm cube voxel phantom to within an acceptable level of uncertainty is, computationally, very challenging. Future work will aim to optimize the phantom and beam modelling parameters to successfully score dose in a high spatial resolution, ZnS-based virtual phantom to validate the dosimetric characteristics of the proposed detector design.

CONCLUSIONS

Previous investigations focused predominantly on clinical linear accelerator treatment head modelling and ISD characterization in the MV range. In the current study we have extended our focus to modelling kV beams in small animal irradiators and investigating the dose perturbations by ISDs. The level of dose absorption in the high-density active volume was found to be significant for gadox and ZnS based models. This leads to significant dose-shadowing in the media behind the phosphor, with respect to the beam direction. If ISDs are going to be used routinely in kilovoltage clinical dosimetry procedures, it is vital that their dose perturbation effects are characterized and mitigated. We have proposed an optimized ISD design which utilizes the higher light yield of the less perturbing ZnS:Ag phosphor to allow for a smaller high-density active volume, significantly mitigating the perturbation of dose in kV radiation fields. Future efforts will focus on the successful and repeatable fabrication of such a detector and the validation of its dosimetric characteristics using measurements and MC-based simulations.

ACKNOWLEDGEMENTS

The authors wish to acknowledge the Irish Centre for High-End Computing (ICHEC) for the provision of computational facilities and support. We would also like to acknowledge funding through the Walton Scholarship of the CAMPEP accredited M.Sc. in Medical Physics at the NUI Galway.

REFERENCES

[1] Alharbi, M., Martyn, M., Chen, L., Gillespie, S., Woulfe, P., O'Keeffe, S. and Foley, M., "Novel optical fibre sensors and their applications in radiotherapy," Proc. SPIE **10680**, 106800Z (2018).

[2] Alharbi, M., Gillespie, S., Woulfe, P., McCavana, P., Keeffe, S. O. and Foley, M., "Dosimetric Characterization of an Inorganic Optical Fiber Sensor for External Beam Radiation Therapy," IEEE Sens. J. **19**(6), 2140–2147 (2019).

[3] Alharbi, M., Martyn, M., O'Keeffe, S., Therriault-Proulx, F., Beaulieu, L. and Foley, M., "Benchmarking a novel inorganic scintillation detector for applications in radiation therapy," Phys. Med. **68**, 124–131 (2019).

[4] Woulfe, P., Sullivan, F. J., Lewis, E. and O' Keeffe, S., "Plastic optical fibre sensor for in-vivo radiation monitoring during brachytherapy," Proc. SPIE **9634**, 96342I (2015).

[5] O'Shea, T. P., Foley, M. J., Rajasekar, D., Patrick, A., van der Putten, W., Moore, M. and Shearer, A., "Electron beam therapy at extended source-to-surface distance: a Monte Carlo investigation," J. Appl. Clin. Med. Phys. **9**(4), 57–67 (2008).

[6] O' Shea, T. P., Sawkey, D. L., Foley, M. J. and Faddegon, B. A., "Monte Carlo commissioning of clinical electron beams using large field measurements," Phys. Med. Biol. **55**, 4083–4105 (2010).

[7] O' Shea, T. P., Foley, M. J. and Faddegon, B. A., "Accounting for the fringe magnetic field from the bending magnet in a Monte Carlo accelerator treatment head simulation," Med. Phys. **38**(6), 3260–3269 (2011).

[8] O' Shea, T. P., Ge, Y., Foley, M. J. and Faddegon, B. A., "Characterization of an extendable multi-leaf collimator for clinical electron beams," Phys. Med. Biol. **56**, 7621–7638 (2011).

[9] Conneely, E., Alexander, A., Stroian, G., Seuntjens, J. and Foley, M. J., "An investigation into the use of MMCTP to tune accelerator source parameters and testing its clinical application," J. Appl. Clin. Med. Phys. **14**(2), 3–14 (2013).

[10] Conneely, E., Alexander, A., Ruo, R., Chung, E., Seuntjens, J. and Foley, M. J., "Monte Carlo investigation of collapsed versus rotated IMRT plan verification," J. Appl. Clin. Med. Phys. **15**(3), 133–147 (2014).

[11] Martyn, M., Shea, T. P. O., Harris, E., Bamber, J., Gilroy, S. and Foley, M. J., "A Monte Carlo study of the effect of an ultrasound transducer on surface dose during intrafraction motion imaging for external beam radiation therapy," Med. Phys. **44**(10), 5020–5033 (2017).

[12] Martyn, M., O'Shea, T., Harris, E., Bamber, J., Gilroy, S. and Foley, M., "Monte Carlo investigation of the dosimetric effect of the Autoscan radiotherapy," Proc. SPIE **9790**, 97900N (2016).

[13] Alharbi, M., Martyn, M., Gillespie, S., Woulfe, P., O'Keeffe, S. and Foley, M., "Performance of a terbium doped

gadolinium oxysulphide plastic optical fiber sensor in a flattening filter free Carlo simulation," Proc. SPIE **10872**, 108720P (2019).
[14] Byrne, K., Alharbi, M., Esplen, N., Woulfe, P., Keeffe, S., Bazalova Carter, M. and Foley, M., "Initial evaluation of the performance of novel inorganic scintillating detectors for small animal irradiation dosimetry," IEEE Sens. J. (2020).
[15] van Eijk, C. W. E., "Inorganic scintillators in medical imaging," Phys. Med. Biol. **47**, R85–R106 (2002).
[16] Johnstone, C. D. and Bazalova-carter, M., "MicroCT imaging dose to mouse organs using a validated Monte Carlo model of the small animal radiation research platform (SARRP)," Phys. Med. Biol. **63**(115012), 14pp (2018).
[17] Yanagida, T., "Inorganic scintillating materials and scintillation detectors," Proc. Jpn. Acad., Ser. B, Phys. Biol. Sci. **94**(2), 75–97 (2018).
[18] Knoll, G., [Radiation Detection and Measurement], John Wiley & Son's (2010).
[19] Weber, M. J., "Inorganic scintillators: today and tomorrow," J. Lumin **100**, 35–45 (2002).
[20] Kubista, M., Sjöback, R., Eriksson, S. and Albinsson, B., "Experimental Correction for the Inner-filter Effect in Fluorescence Spectra," Analyst **119**(3), 417–419 (1994).
[21] Wong, J., Armour, E., Kazanzides, P., Lordachita, I., Tryggestad, E., Deng, H., Mantinfar, M. and Kennedy, C., "A high resolution small animal radiation research platform (SARRP) with x-ray tomographic guidance capabilities," Int. J. Radiat. Oncol. Biol. Phys. **71**(5), 1591–1599 (2008).
[22] Rogers, D. W. O., Walters, B. and Kawrakow, I., "BEAMnrc Users Manual," NRCC Report PIRS-0509(A)revL (2019).
[23] Rogers, D. W. O. and Mackie, T. R., "BEAM: A Monte Carlo code for simulating radiotherapy units," Med. Phys. **22**(5), 503–524 (1994).
[24] Bazalova, M., Zhou, H., Keall, P. J. and Graves, E. E., "Kilovoltage beam Monte Carlo dose calculations in submillimeter voxels for small animal radiotherapy," Med. Phys. **36**(11), 4991–4999 (2009).
[25] Walters, B., Kawrakow, I. and Rogers, D. W. O., "DOSXYZnrc Users Manual," 1–132 (2019).
[26] Duane, S., Bielajew, A. F. and Rogers, D. W. O., "Use of ICRU-37/NBS Collision Stopping Powers in the EGS4 System," NRCC Report, PIRS-0173 (1989).
[27] McGowan, H. C. E., Faddegon, B. A. and Ma, C.-M., "STATDOSE for 3D dose distributions," NRCC Report PIRS-0509(F) (2020).